

Abstract

One-way wavefield extrapolation operators are used to propagate acoustic wavefields from one depth level to another. Applying the extrapolation in a recursive way, using small depth steps, demands that the operators do not amplify the wavefield at every depth step. Previously a weighted least squares technique has been described to estimate short, stable and accurate forward and inverse wavefield extrapolation operators. This technique produced accurate extrapolation operators which were comparable with the results of other known techniques like the Remez exchange and non-linear optimization method. In this paper the weighted least squares (WLSQ) technique is refined by using different model functions. In using those functions the extrapolation operators can be made more accurate and can also be tailored for special purposes, such as asymmetric operators. Zero-offset migration impulse responses are shown in 2D media and the Sigsbee2A data set is used to illustrate the usage of the extrapolation operators in pre-stack depth migration.

Introduction

Recursive wavefield extrapolation in the frequency domain extrapolates data from depth level z_m to level z_{m+1} , where $\Delta z = |z_{m+1} - z_m|$ is small compared to the operator length. Due to the recursive use of the operators special care must be taken about the amplitudes. An amplitude larger than 1 can lead to unstable extrapolation results, while an amplitude smaller than 1 will attenuate the wavefield during extrapolation.

In the $k_x - \omega$ domain the extrapolation operator for a 2-dimensional medium is given by the following equation;

$$\tilde{W}(k_x, \omega, \Delta z) = \exp(-jk_z \Delta z), \quad (1)$$

with $k_z = \sqrt{k^2 - k_x^2}$, $k = \frac{\omega}{c}$, ω the angular frequency and c the propagation velocity. Wavefield P is extrapolated one depth step by

$$\tilde{P}(k_x, \omega, z_{m+1}) = \tilde{W}(k_x, \omega, z_{m+1} - z_m) \tilde{P}(k_x, \omega, z_m). \quad (2)$$

The analytical inverse Fourier transform of equation (1) is a scaled Hankel function, see Berkhout (1984):

$$W(x, \omega, \Delta z) = -jk \frac{\Delta z}{2r} H_1^{(2)}(kr) \quad (3)$$

with $r = \sqrt{x^2 + \Delta z^2}$ and $H_1^{(2)}(kr) = J_1(kr) - jY_1(kr)$ is the first-order Hankel function of the second kind. The cheapest way to obtain a short operator in the space domain is by discretization of equation (3) and truncating it to a finite number of points. The accuracy of the resulting short operator can be assessed by comparing its spectrum with equation (1).

In Figure 1a the amplitude of the wavenumber spectrum of the operator of equation (3), truncated to 25 points, is shown together with the amplitude of the phase-shift operator $\tilde{W}(k_x, \omega, \Delta z)$ (solid line). Note that the wavenumber spectrum of the truncated operator is significantly larger than 1 for $|k_x| \leq k$. Recursive application of this operator causes that waves are amplified at every extrapolation step, which in the end 'blows up' the extrapolation result. Note that, since extrapolation is always done for a finite (but large) number of steps, amplitudes slightly larger than 1 are allowed. We consider an operator to be conditionally stable when its amplitude is smaller than 1.001 for all wavenumbers. In a homogeneous medium and a single frequency this leads to, after 500 extrapolation steps, a maximum amplification of 1.65.

Figure 1b shows an operator which has been optimized using the Remez exchange algorithm (Soubaras, 1996). Figure 1c and 1d are the result of WLSQ optimization and will be discussed in more detail below.

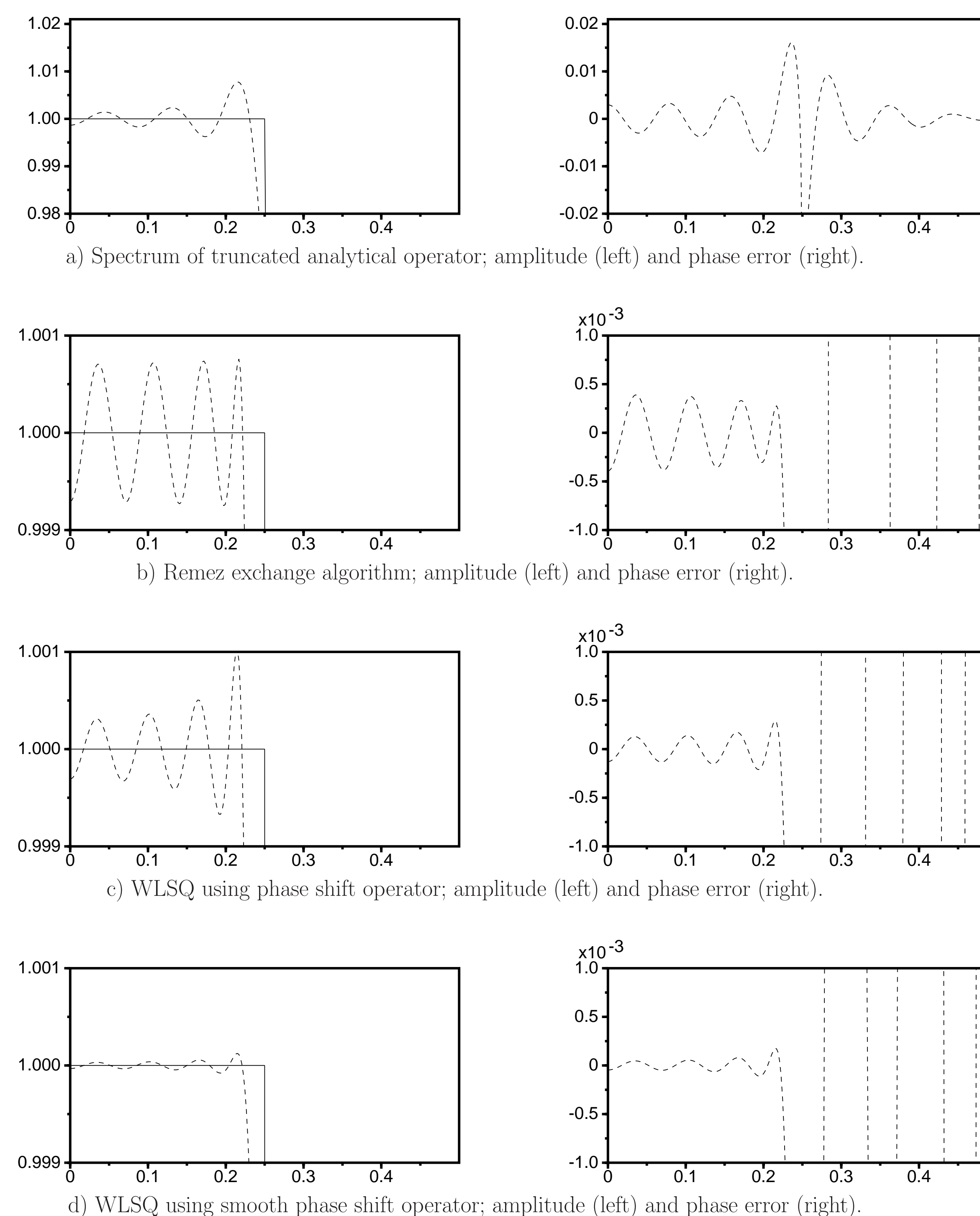


FIGURE 1: Comparison between spectra of different designed wave field extrapolation operators. For each operator $k = \frac{\omega}{c} = \frac{k_{N_{\text{opt}}}}{2}$. Since the operators are symmetric, only the right half is shown. The effect of the truncation of the analytical operator can be seen in the wavenumber amplitude and phase spectrum given in a). The result after optimization with the Remez exchange algorithm is shown in b). Figure c) shows WLSQ optimization with the model function \tilde{W} being equal to the phase-shift operator and d) using a smooth version of \tilde{W} given by equation (7b). Note the vertical scale difference between Figure a and Figures b, c and d. For all these figures we have chosen: an operator length of 25 points, $\Delta x = 10\text{m}$, $\Delta z = 2\text{m}$, $\omega = 50\pi$ radians/s, $N = 512$ samples, $c = 1000$ m/s and the maximum propagation angle at $\alpha_{\text{max}} = 75^\circ$. The horizontal axis represents normalized wavenumber cycles ($\frac{x}{N}$).

Weighted Least Squares

The goal in the optimization procedure is to obtain a short spatial convolution oper-

ator, which has a wavenumber spectrum over a desired wavenumber band, equal or close to the exact formulation in the frequency-wavenumber domain. This problem can be written as an integral equation

$$\tilde{W}(k_x) = \int_{-x_1}^{x_1} \exp(jk_x x) W(x) dx \quad \text{for } \|k_x\| \leq k_N, \quad (4)$$

where $W(x)$ is the (unknown) convolution operator. In this integral equation, the integration is carried out over a limited spatial interval, representing the short operator. Also the frequency-wavenumber domain of the operator is band-limited. The discrete counterpart of this integral is given by

$$\tilde{W} = \Gamma W \quad (5)$$

The weighted least squares (WLSQ) solution of matrix equation (5) is given by

$$W_{\text{opt}} = [\Gamma^H \tilde{\Lambda} \Gamma]^{-1} \Gamma^H \tilde{\Lambda} \tilde{W}. \quad (6)$$

$\Gamma^H \tilde{\Lambda} \Gamma$ is a square $M \times M$ matrix, which has to be inverted to solve for the unknown. For 1-dimensional operators this matrix has a Toeplitz structure and can be inverted efficiently using the Levinson scheme. If in equation (6) the weight matrix is chosen identical to the unit matrix $\tilde{\Lambda} = \mathbf{I}$, then the right hand side of equation (6) is an inverse Fourier transform of N -points, which is truncated to M -points in the spatial domain. In this specific case no optimization is carried out.

For accurate extrapolation results the desired operator \tilde{W} must be equal to the phase-shift operator for the propagating waves, however the behavior outside this part can differ from the phase-shift operator. A so-called smooth operator has been designed in such a way that outside the band of interest the amplitude and the phase are defined by a cubic spline, which goes smoothly to zero:

$$\|\tilde{W}(k_x, \omega, \Delta z, \alpha)\| = \begin{cases} 1.0 & |k_x| \leq k \sin(\alpha) \\ \text{spline} & |k_x| > k \sin(\alpha) \\ 0 & |k_x| = \frac{\pi}{\Delta x} \end{cases} \quad (7a)$$

$$\arg(\tilde{W}(k_x, \omega, \Delta z, \alpha)) = \begin{cases} -jk_z \Delta z & |k_x| \leq k \sin(\alpha) \\ \text{spline} & |k_x| > k \sin(\alpha) \\ 0 & |k_x| = \frac{\pi}{\Delta x} \end{cases} \quad (7b)$$

where α is the maximum propagation angle of interest. The weight function is box-shaped. By using this smoother objective function the least-squares algorithm can find a smoother solution and is in turn better constraint.

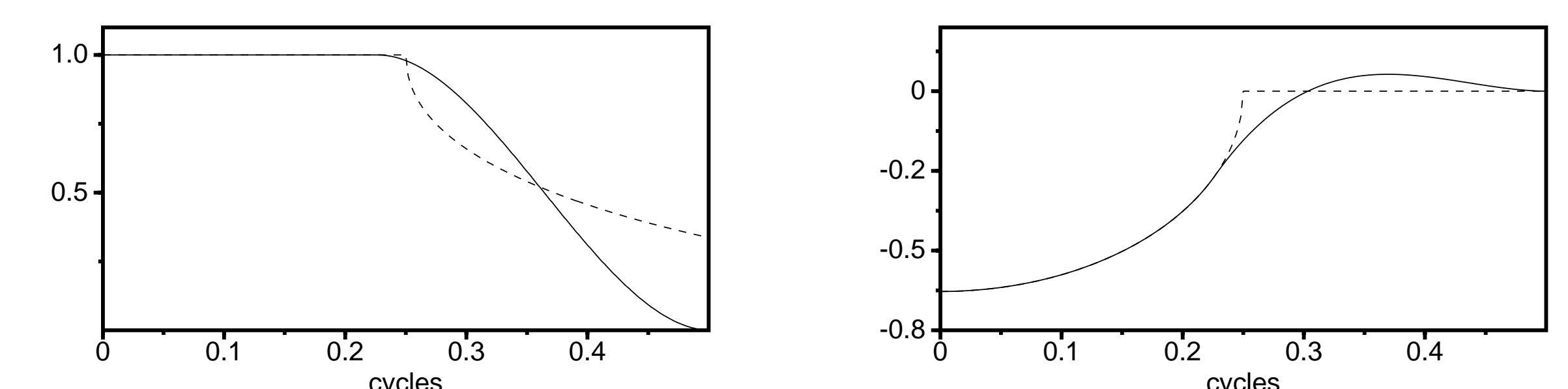


FIGURE 2: Amplitude and phase of phase-shift operator (dotted line) and the smooth version of the phase-shift operator.

The WLSQ optimized convolution operator, based on an object function equal to the phase-shift operator, is shown in Figure 1c. The wavenumber spectrum is stable for all wavenumbers and is accurate within the band of interest. The accuracy of this operator is the same as the operators of Holberg (1988) and Blacquiere et.al. (1989). Figure 1d shows the WLSQ optimized operator with the smooth object function. The operator designed with the smoother version has clearly lower amplitude oscillations.

Migration examples

To test the accuracy of the extrapolation operators zero-offset migration experiments are carried out. In these experiments a 19 points extrapolation operator in a homogeneous medium with a velocity of 2000 m/s, a receiver length of 2000 m and a maximum extrapolation depth of 1000 m with $\Delta x = 10$, $\Delta z = 2$ m is used. The zero-offset trace in the middle of the shot record contains three Ricker wavelets at 0.3, 0.6 and 0.9 s, all the other traces are filled with zeros. The source wavelet is sampled with 4 ms and has a frequency peak at 30 Hz.

Figure 3a shows the impulse responses for a non-recursive reference result. Operators designed with the equiripple approach of the Remez algorithm are shown in (3b), the WLSQ operators based on the phase-shift operator in (3c) and WLSQ operators based on the smooth phase-shift operator in (3d). The smooth operator result has on average the least numerical artifacts. However, at the higher angles (above 80°) the smooth operator has slightly more and stronger artifacts.

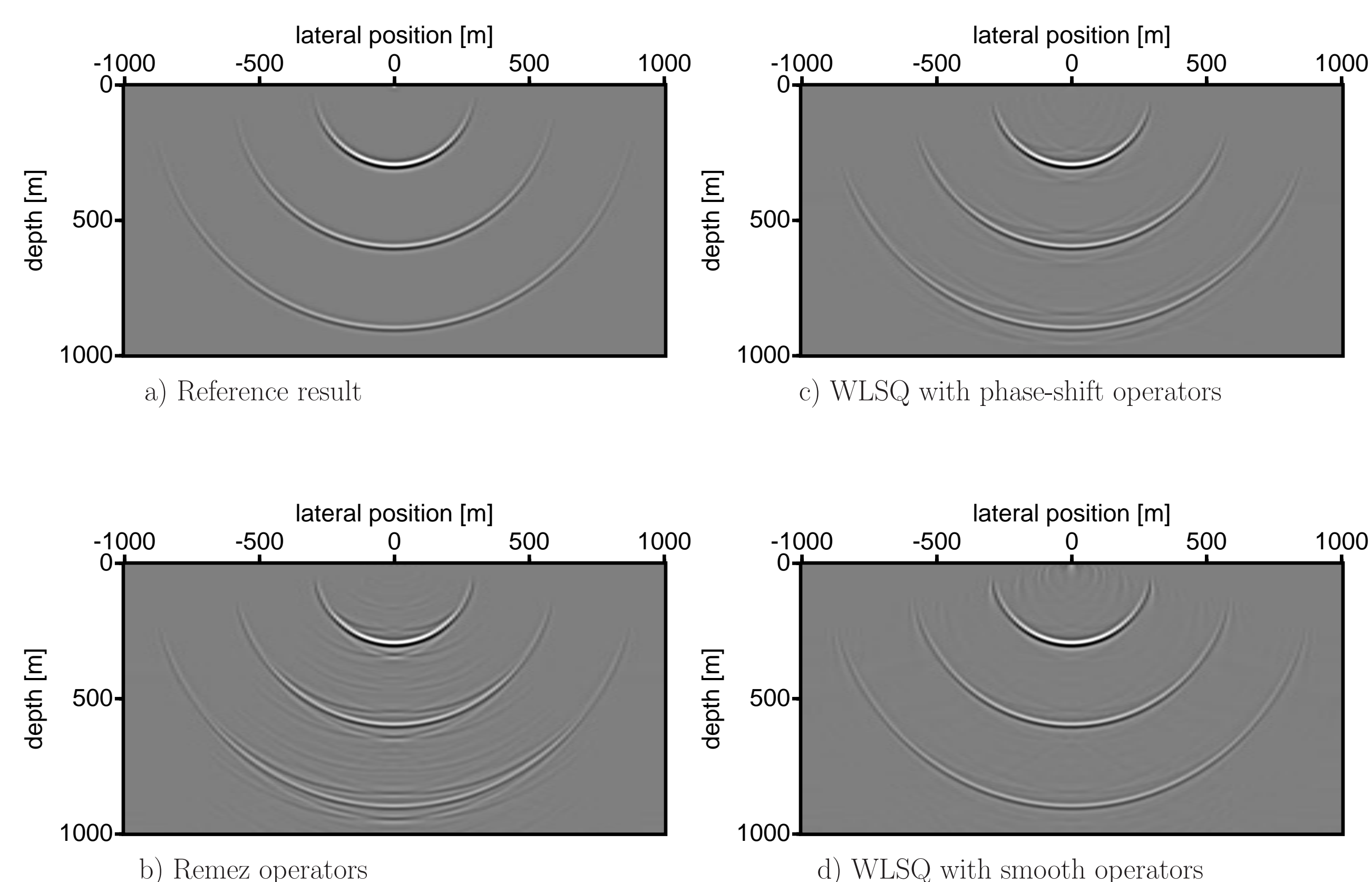


FIGURE 3: Migration impulse responses for a non-recursive reference result (a) and three recursive methods using: Remez exchange optimized operators (b), WLSQ based on phase-shift operator (c) and WLSQ based on the smooth phase-shift operator (d). The impulse responses are modeled with a frequency range of (0-80) Hz, $\Delta t = 4$ ms, $\Delta x = 10$ m, $\Delta z = 2$ m, a velocity of 2000 m/s and an operator length of 19 points.

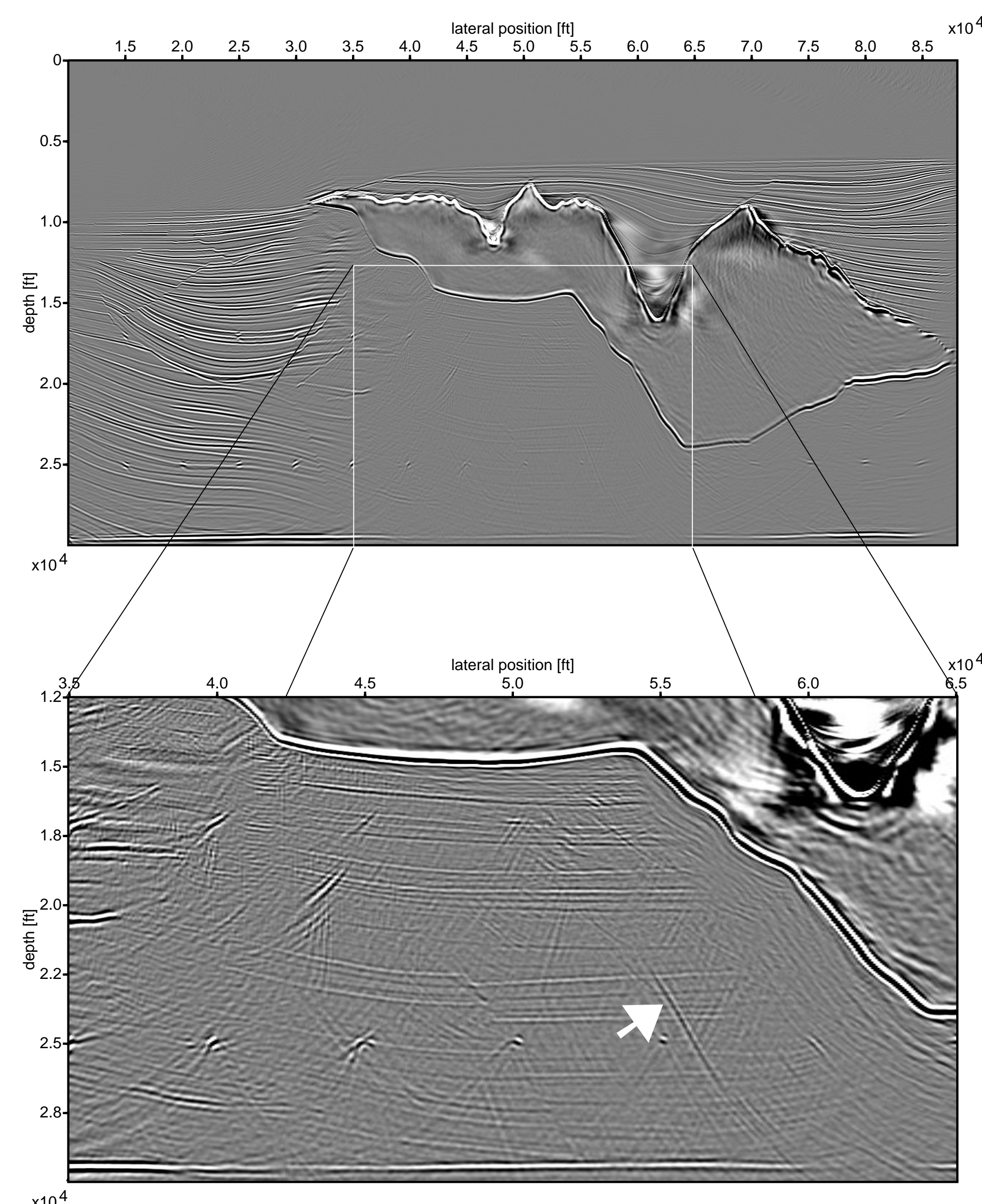


FIGURE 4: Pre-stack depth migration of Sigsbee2A data set with optimized WLSQ operators with a fixed length of 25 points. The bottom picture is a zoom of the area below the salt. The transmission coefficients through the salt are not taken into account, giving a lower amplitude image below the salt compared to the surrounding areas. Most events below the salt are imaged, only the turning waves are not imaged correctly. In the zoomed area along the right side of the salt bottom there is a large shadow zone. In this shadow zone only the diffracting point at (60000,25000) is partly imaged.

The Sigsbee2A data set (Glogovsky et al., 2002) is depth migrated using one fixed operator length of 25 points, but with a search done for the best operator as function of the weight factor. The pre-stack depth migration result is shown in Figure 4. The steep faults beside the salt structure are imaged correctly. In the zoom area below the salt, all events that contain reflection energy are clearly visible. Close to the right steep bottom of the salt there are no layers visible due to an illumination problem

caused by the salt structure and the chosen acquisition geometry. An internal multiple of the salt body (indicated by an arrow) has been imaged as a steep ghost fault crossing the layers.

The disadvantage of one-way migration is that it is not possible to handle turning/bending waves in the recursive migration (for propagation angles larger than 80°). Also the transmission coefficients are not included, resulting in lower amplitude, but structural still accurate, images below the salt.

Conclusions

In this paper the weighted least squares technique has been further improved by using a smooth object function in the estimation of extrapolation operators. The presented results indicate that these improved operators give very accurate extrapolation results. The WLSQ algorithm used to compute the operators is very fast and multiple evaluations for different weight functions and operator lengths makes it possible to search for the best operator with minimum operator length and smallest amplitude below a certain threshold.

The WLSQ is not only suited for extrapolation operator design, but can also be used in other filter design problems for an efficient and controlled transformation of the (smoothed) operator in the Fourier domain back to a convolution operator in the original domain.

The extension of the WLSQ technique for 2 dimensional operators, to be used in 3 dimensional media is straightforward as discussed by Thorbecke and Berkhou (1994).

Acknowledgments

We would like to thank the research school ISES and the Atlss project of the European Union for supporting this research.

References

- Berkhout, A. J. (1984). *Seismic resolution: resolving power of acoustic echo techniques*. Geophysical Press Ltd.
- Blacquièrè, G., Debeye, H. W. J., Wapenaar, C. P. A., and Berkhout, A. J. (1989). 3D table-driven migration. *Geophys. Prosp.*, 37(08):925–958.
- Glogovsky, V., Landa, E., and Paffenholz, J. (2002). Integrated approach to subsalt depth imaging: Synthetic case study. volume 21, pages 1217–1223.
- Holberg, O. (1988). Towards optimum one-way wave propagation. *Geophys. Prosp.*, 36(02):99–114.
- Soubaras, R. (1996). Explicit 3-D migration using equiripple polynomial expansion and Laplacian synthesis. *Geophysics*, 61(05):1386–1393.
- Thorbecke, J. W. and Berkhout, A. J. (1994). 3-D recursive extrapolation operators: An overview. In *64th Annual Internat. Mtg., Soc. Expl. Geophys., Expanded Abstracts*, pages 1262–1265. Soc. Expl. Geophys.